JCTC Journal of Chemical Theory and Computation

Article

pubs.acs.org/JCTC

Effect of Heterojunction on Exciton Binding Energy and Electron–Hole Recombination Probability in CdSe/ZnS Quantum Dots

Jennifer M. Elward[†] and Arindam Chakraborty*[,‡]

[†]Army Research Laboratory, Aberdeen Proving Ground, Aberdeen, Maryland 21005, United States

[‡]Department of Chemistry, Syracuse University, Syracuse, New York 13244, United States

ABSTRACT: Presence of heterojunctions is important for generation of free charge carriers and the dissociation of bound electron–hole pairs in semiconductor nanoparticles. This work presents a theoretical investigation of the effect of core/shell heterojunction on electron–hole interaction in CdSe/ZnS quantum dots. The excitonic wave function in the CdSe/ZnS dots was calculated using the electron–hole explicitly correlated Hartree–Fock (eh-XCHF) method and the effect of successive addition of the ZnS shell on exciton binding energy, electron–hole recombination probability, and the electron–hole separation distance was investigated. It was found that the scaling of all the three quantities as a function of dot diameter did not follow conventional volume scaling laws of core-only dots, and the scaling laws were significantly altered due to the presence of the heterojunction. The spatial localization of the quasiparticles in the core/shell quantum dot was analyzed by calculating the 1-particle reduced density from the eh-XCHF wave function and partitioning the density spatially into core and shell regions. It was found that in the 15 nm CdSe/ZnS dot, the relative probability of the electron localization in the shell region was higher than the hole by a factor of 3. The degree of spatial localization of the quasiparticles was found to depend strongly on the initial size of the CdSe core in the core/shell quantum dot. It was found that a reduction in the CdSe core diameter by a factor of 1.7 resulted in an enhancement of the preferential localization of the electron in the shell region by a factor of 11.3. The results demonstrate that large CdSe/ZnS quantum dots with a small CdSe core have the necessary characteristics for efficient exciton dissociation and generation of free charge carriers.

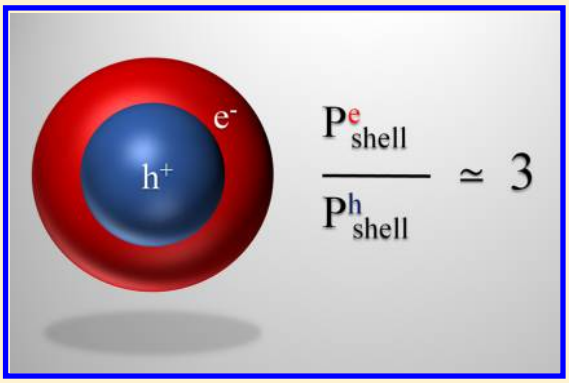

1. INTRODUCTION

Over the past decade there has been increased research interest in semiconductor nanocrystals such as quantum dots (QDs) due to their inherently tunable properties. Controlling the particle shape,[1−3] size,[4,5] and material composition[6−10] allow for direct manipulation of optical and electronic properties of QDs. Applications of nanoparticles include labeling and tracking of biomolecules,[11−18] light emitting devices,[19−22] hydrogen generation,[23−26] resonance energy transfer,[27−31] and photovoltaics.[32−46]

Electronic excitations in QDs can be represented in quasiparticle representation by formation of electron–hole (eh) pairs (excitons). Generation and dissociation of excitons and multiexcitons[47−51] have important applications in solar-to-electric and solar-to-chemical energy conversion processes.[52,53] Theoretical investigation of these processes requires accurate treatment of electron–hole correlation in QDs. One of the metrics used for studying eh-interaction is the exciton binding energy,[54−57] which is defined as the energy required to dissociate the bound eh-pair. Both exciton binding energy and finite excitonic lifetime can be modified by changing the chemical composition and dot size.[54−62]

There is also technological interest in designing QDs for controlling charge separation, which can be achieved by changing the size of the QD, modifying the shape, and introducing a heterojunction into the system.[63−65] Core/shell quantum dots are ideal for applications that require transfer of charge carriers to an outside sink for photovoltaic applications. When the shell is grown on a core material, the electronic structure of the host material is modified and this introduces new features into the electronic and optical properties of the material. Based on the band alignment between the core and shell material, the interface can be classified as a type I, type II, or quasi-type II heterojunction.[66] The optical and charge transport properties can be modified significantly by changing the shell thickness of the nanoparticle and have been used in experimental studies for controlling charge separation,[67−69] hole-transfer,[70] and electron-transfer rates.[71]

In addition to experimental studies, theoretical approaches have been used to study electron–hole interactions in chemical systems for photovoltaic applications.[72−76] For smaller quantum dots, an all-electron treatment can be used with methods like density functional theory (DFT),[77−85] GW–Bethe–Salpeter,[86−88] many-body perturbation theory,[89,90] and reduced-density matrix method.[91−95] However, treatment of

Received: June 27, 2014
Published: January 3, 2015

DOI: 10.1021/ct500548x
J. Chem. Theory Comput. 2015, 11, 462−471

larger quantum dots becomes computationally prohibitive with all-electron theoretical methods, and traditionally, atomistic semiempirical pseudopotential methods have been used to address this problem.[54,57,96−99]

In this work, we have investigated the effect of the heterojunction on a series of CdSe/ZnS quantum dots with diameters 5−15 nm. The excitonic wave function was obtained using the electron−hole explicitly correlated Hartree−Fock (eh-XCHF) method, and the exciton binding energy, electron−hole recombination probability, and electron−hole separation distance were computed for each dot in the series. Effect of shell thickness, core-size, and dot diameter on the excitonic properties were analyzed, and preferential spatial localization of the quasiparticles was investigated using the 1-particle reduced density. The results from this multifaceted study show that the presence of the heterojunction can promote exciton dissociation and generation of free charge carriers.

The remainder of the paper is organized as follows. The theoretical and computational implementation details of the eh-XCHF method are summarized in Section 2. The results from the calculations are presented in Section 3, and the conclusions are provided in Section 4.

2. THEORY

2.1. Form of the Electron−Hole Wave Function. The electronically excited quantum dot was described using the electron−hole Hamiltonian that has been used successfully[100−111] for characterizing electron−hole interaction in nanoparticles.

$$H = \sum_{ij} \langle i|\frac{-\hbar^2}{2m_e}\nabla_e^2 + v_{ext}^e|j\rangle e_i^\dagger e_j + \sum_{ij} \langle i|\frac{-\hbar^2}{2m_h}\nabla_h^2 + v_{ext}^h|j\rangle h_i^\dagger h_j + \sum_{iji'j'} \langle iji'j'|\varepsilon^{-1}r_{eh}^{-1}|iji'j'\rangle e_i^\dagger e_j h_{i'}^\dagger h_{j'} + \sum_{ijkl} w_{ijkl}^{ee} e_i^\dagger e_j^\dagger e_l e_k + \sum_{ijkl} w_{ijkl}^{hh} h_i^\dagger h_j^\dagger h_l h_k \quad (1)$$

The external potential v_{ext} in the above expression depends on positions of all the atoms in the quantum dot and can be calculated using either DFT[77−85] or atomistic pseudopotential method.[54,57,96−99] We are interested in QDs with diameter in the range 5−15 nm and performing eh-XCHF calculation with atomistic pseudopotential for these large QDs is computationally prohibitive because of large number of atoms in the systems. To overcome the computational bottleneck and to make the calculations feasible, we have approximated the external potential by the parabolic confinement potential, which has been successfully used for calculating optical and electronic properties of nanoparticles.[112−121] The confining potential for the electrons and holes was described using the following expression,

$$v_{ext}^\alpha = \frac{1}{2}k_\alpha|\mathbf{r}_\alpha|^2 + v_{mat}^\alpha \quad \alpha = \text{e, h} \quad (2)$$

where the force constants, k_α, for the parabolic potential were obtained from ref 122. These force constants were determined using a particle-number based search procedure. The key idea of the method is to find an external potential that ensures that the single particle electron and hole densities are confined in the volume of the quantum dot. The force constant, k_α, was obtained via the following minimization procedure,

$$\min_{k_\alpha^{min}}(N_\alpha - \int_0^{D_{dot}/2} dr r^2 \int d\Omega \rho_\alpha(\mathbf{r})[v_{ext}^\alpha])^2 \quad (3)$$

where α = e, h; $d\Omega = \sin\theta d\theta d\phi$; D_{dot} is the dot diameter; and k_α^{min} is the smallest force constant that satisfies the above minimization condition.

In addition to the parabolic confinement potential, a material potential was used to describe the core and shell regions

$$v_{mat}^\alpha = v_{CdSe}^\alpha + m(r - r_{core})(v_{ZnS}^\alpha - v_{CdSe}^\alpha) \quad (4)$$

where α = e, h. A masking function[97] $m(r)$ was used to transition smoothly between the core and shell materials. This masking function is analogous to the one developed by Franceschetti et al. for smoothly connecting regions of different dielectric functions in quantum dots.[97] The function used in the present work is given by the following expression

$$m(r) = \frac{(\tanh(\beta r) + 1)}{2} \quad (5)$$

where β is a parameter used to control smoothness between core and shell region and is given in Table 1.

Table 1. Material Parameters for the CdSe/ZnS Quantum Dots Used in the Electron−Hole Hamiltonian[a]

property	value CdSe	value ZnS
m_e	0.13	0.25
m_h	0.38	1.30
ε	6.20	8.90
v_{mat}^e	−0.147	−0.114
v_{mat}^h	−0.209	−0.176
β	10.0	10.0

[a]All values are given in atomic units.

The optical properties of the quantum dots were calculated using the electron−hole explicitly correlated Hartree−Fock method (eh-XCHF).[123,124] The electron−hole wave function was represented by multiplying the electron and hole Slater determinants by an explicitly correlated function, as shown in the following expression,

$$\Psi_{XCHF} = G\Phi^e\Phi^h \quad (6)$$

We have used the Gaussian-type geminal function (GTG) as the explicitly correlated function that is defined in the following equation

$$G(\mathbf{r}^e, \mathbf{r}^h) = \sum_{i=1}^{N_e}\sum_{j=1}^{N_h}\sum_{k=1}^{N_g} b_k \exp[-\gamma_k r_{ij}^2] \quad (7)$$

where N_e and N_h are number of electrons and holes and N_g is the number of Gaussian-type geminals in the expansion. The GTG includes the electron−hole interparticle distance directly into the form of the wave function. The b and γ parameters of the GTG function were determinedvariationally by minimizing the total energy.

The eh-XCHF wave function was obtained from variational minimization of the eh-XCHF energy,

$$E_{eh\text{-}XCHF} = \min_{G,\Phi^e,\Phi^h} \frac{\langle\Psi_{eh\text{-}XCHF}|H|\Psi_{eh\text{-}XCHF}\rangle}{\langle\Psi_{eh\text{-}XCHF}|\Psi_{eh\text{-}XCHF}\rangle} \quad (8)$$

The minimization was performed by first performing congruent transformation[125,126] on the Hamiltonian and then

DOI: 10.1021/ct500548x
J. Chem. Theory Comput. 2015, 11, 462−471

solving the coupled electron−hole self-consistent field (SCF) equations[127] as shown below,

$$\mathbf{F}_G^{\mathrm{e}}[\mathbf{C}^{\mathrm{h}}]\mathbf{C}^{\mathrm{e}} = \lambda^{\mathrm{e}}\mathbf{S}_G^{\mathrm{e}}\mathbf{C}^{\mathrm{e}} \tag{9}$$

$$\mathbf{F}_G^{\mathrm{h}}[\mathbf{C}^{\mathrm{e}}]\mathbf{C}^{\mathrm{h}} = \lambda^{\mathrm{h}}\mathbf{S}_G^{\mathrm{h}}\mathbf{C}^{\mathrm{h}} \tag{10}$$

In the above expression, $\mathbf{F}_G^{\mathrm{e}}$ and $\mathbf{F}_G^{\mathrm{h}}$ are the Fock matrices for the electron and hole, respectively. The subscript G denotes that the Fock operators were obtained from the congruent-transformed Hamiltonian and include contribution from the geminal operator. Equations 6−10 represent the key steps of the eh-XCHF method that are relevant to the present work. The detailed derivation of the eh-XCHF method, and the computational details of construction of the Fock matrix and evaluation of the integrals involving the GTG correlation function have been derived earlier[123,124,127] and are not repeated here. The eh-XCHF method has been successfully used in previous work[122] for calculation of optical properties of quantum dots and was used in the present work for obtaining accurate results at an affordable computational cost.

There are two important advantages associated with using the Gaussian-type geminal function in the eh-XCHF wave function. First, the variational determination of the geminal parameters results in an accurate description of the wave function in the neighborhood of the electron−hole coalescence point. This feature has been shown to be important for accurate computation of both exciton binding energy and eh-recombination probability.[122] Second, the presence of the GTG function can alleviate the need for a large CI expansion for treating electron−hole correlation.[125] This can be seen by relating the eh-XCHF wave function to an infinite-order CI expansion as shown in the following equation

$$G|\Psi_0\rangle = \underbrace{\sum_{ii'}^{\infty} |\Phi_i^{\mathrm{e}}\Phi_{i'}^{\mathrm{h}}\rangle\langle\Phi_i^{\mathrm{e}}\Phi_{i'}^{\mathrm{h}}|G|\Psi_0\rangle}_{1} \tag{11}$$

In the above expression, the CI coefficients are not independent variational parameters but are constrained by the form of the correlation function G.

2.2. Computational Details. The material parameters for the CdSe core-only and CdSe/ZnS core/shell quantum dots used in the electron−hole Hamiltonian are summarized in Table 1. These parameters were taken from refs 57, 128, and 129. The single particle basis for the electron and hole were constructed as a linear combination of Gaussian-type orbitals functions, as shown in the following expression,

$$\Phi^{\alpha} = \sum_{i=1}^{n_b} c_i\phi_i(\mathbf{r}) \quad \alpha = \mathrm{e},\ \mathrm{h} \tag{12}$$

A linear combination of 10 basis functions was used for each particle with s, p, and d angular momentum values. The exponents α for the GTOs were found by minimizing the single-component energy for electron and hole, respectively. A set of three geminal functions was used for each dot and the geminal parameters $\{b_k, \gamma_k\}$ together with the expansion coefficients $\{c_i\}$ were obtained by minimizing the eh-XCHF equation. To ensure that the eh-XCHF energy is always bounded from above by the mean-field energy, the first geminal parameters were set to $b_1 = 1$ and $\gamma_1 = 0$.

3. RESULTS AND DISCUSSION

3.1. Effect of Shell Thickness in CdSe/ZnS QD. The change in exciton binding energy, eh-recombination probability, and electron−hole separation distance as a function of shell thickness were calculated using the eh-XCHF method. A series of CdSe/ZnS quantum dots with diameters 6−15 nm were investigated by adding ZnS shell to a CdSe core with core-diameter of 4.8 nm. The exciton binding energy E_{BE} was calculated from the difference between the bound and the noninteracting electron−hole pair, as shown the following equation,

$$E_{\mathrm{BE}} = E_0 - E_{\mathrm{eh-XCHF}} \tag{13}$$

where the noninteracting energy E_0 was obtained by minimizing the expectation value of the noninteracting Hamiltonian H_0

$$H_0 = \lim_{V_{\mathrm{eh}}\to 0} H \tag{14}$$

As shown in Figure 1, the exciton binding energy was found to decrease with increasing shell thickness. The exciton binding

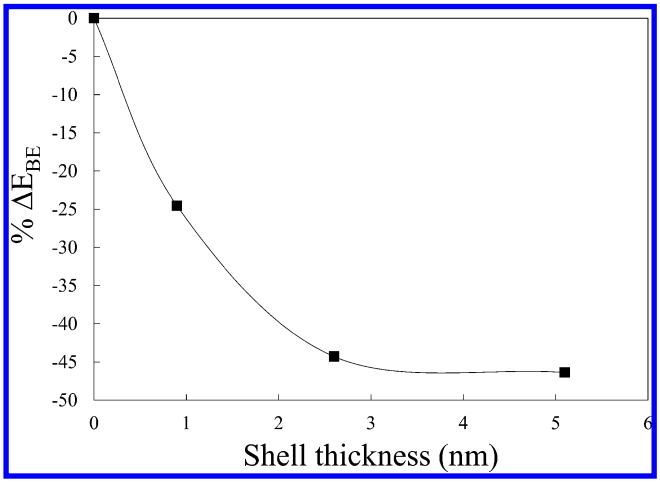

Figure 1. Percent change in exciton binding energy as a function of shell thickness for CdSe/ZnS core/shell quantum dot with core diameter of 4.8 nm. $E_{\mathrm{BE}}^{\mathrm{core}} = 0.264$ eV.

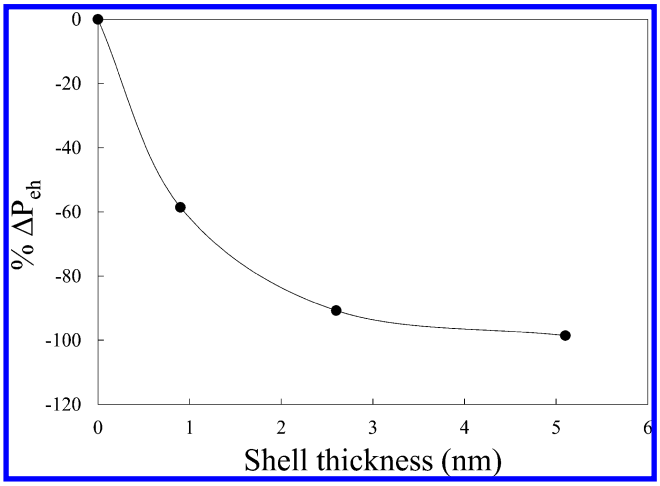

Figure 2. Percent change in electron−hole recombination probability as a function of shell thickness for CdSe/ZnS core/shell quantum dot with core diameter of 4.8 nm.

DOI: 10.1021/ct500548x
J. Chem. Theory Comput. 2015, 11, 462−471

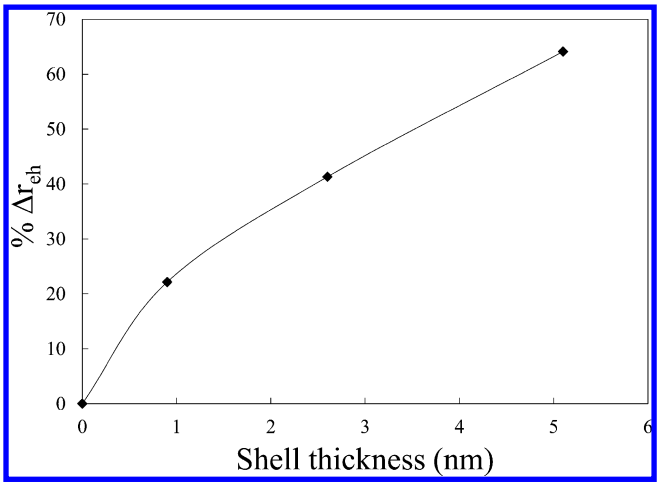

Figure 3. Percent change in electron−hole separation as a function of shell thickness for CdSe/ZnS core/shell quantum dot with core diameter of 4.8 nm. r_{eh}^{core} = 1.18 nm.

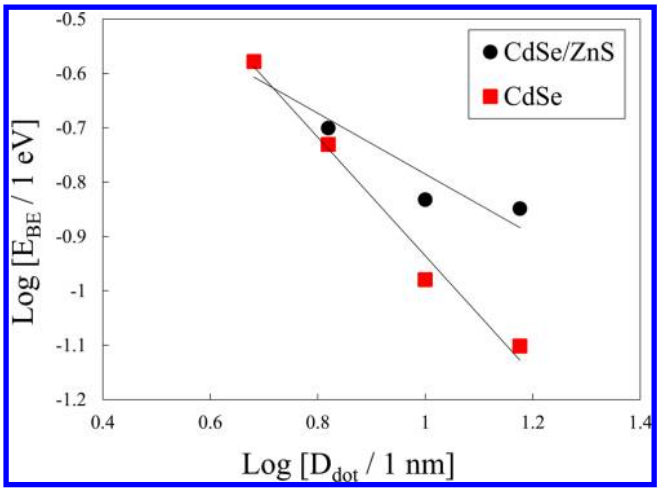

Figure 6. Exciton binding energy as a function of dot size for core-only and core/shell quantum dots. A core diameter of 4.8 nm was used for the CdSe/ZnS quantum dots.

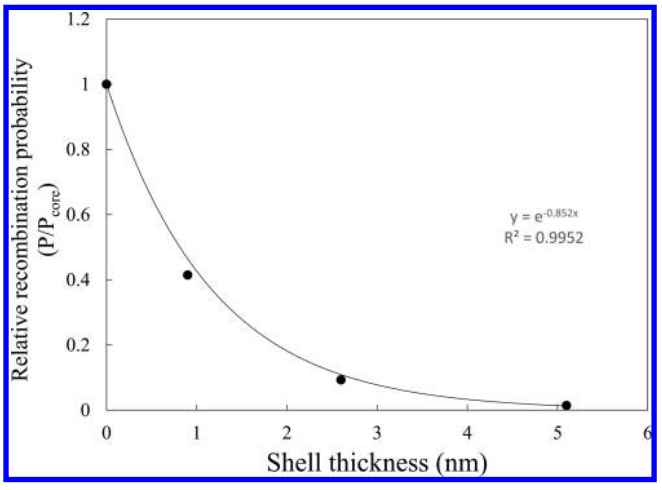

Figure 4. Ratio of recombination probability as a function of ZnS shell thickness for CdSe/ZnS quantum dot with core diameter of 4.8 nm. Exponential fit is given as $y = e^{-0.852x}$.

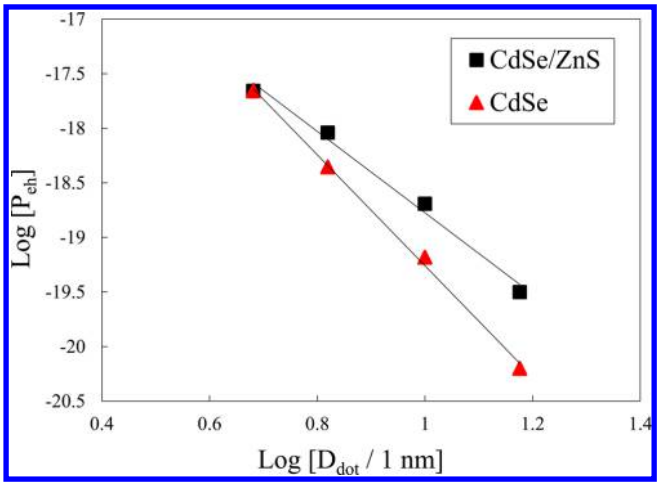

Figure 7. Dependence of recombination probability as a function of dot diameter for core-only and core/shell quantum dots. A core diameter of 4.8 nm was used for the CdSe/ZnS quantum dots.

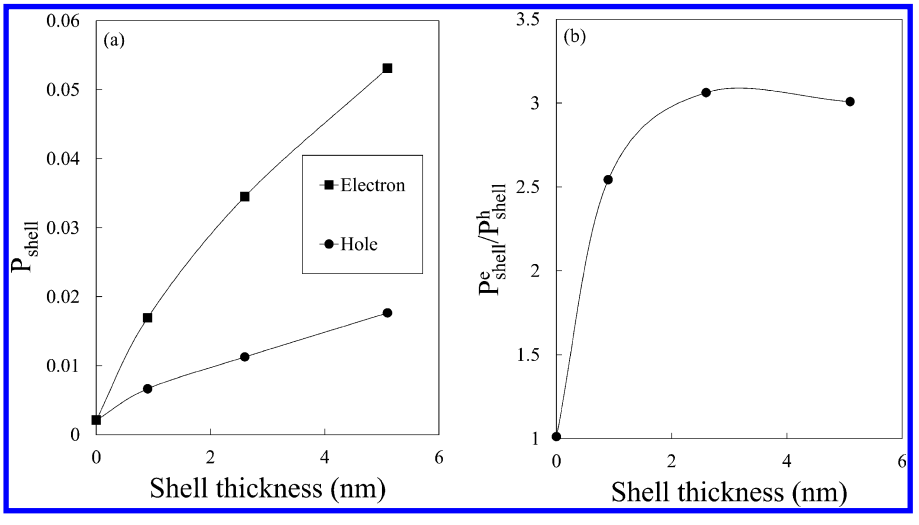

Figure 5. (a) Probability of finding an electron and hole within the shell region and (b) ratio of $P_{shell}^{e}/P_{shell}^{h}$ for a CdSe/ZnS quantum dot with core diameter of 4.8 nm.

DOI: 10.1021/ct500548x
J. Chem. Theory Comput. 2015, 11, 462−471

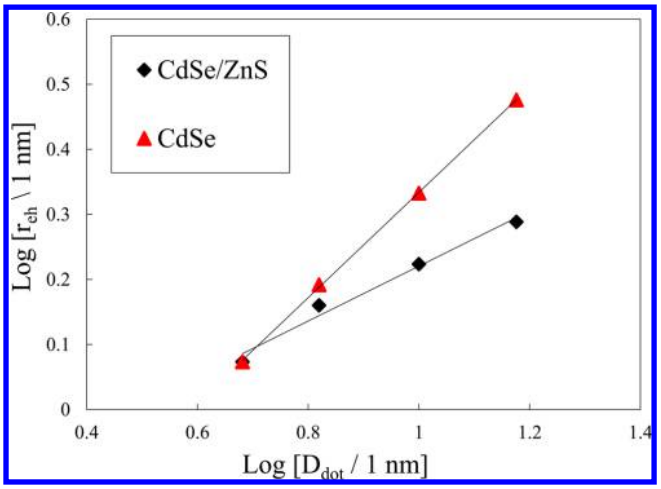

Figure 8. Average electron−hole separation as a function of dot diameter. A core diamter of 4.8 nm was used for CdSe/ZnS quantum dots.

Table 2. Exciton Binding Energy (meV) for the Core/Shell Quantum Dot Systems[a]

dot diam. (nm)	2.8 nm core-diam. (meV)	4.8 nm core-diam. (meV)
4.8	290	
6.6	270	199
10.0	202	147
15.0	186	142

[a]The core-only E_{BE} for the 2.8 nm core and 4.8 nm core are 447.7 and 264.2 meV, respectively.

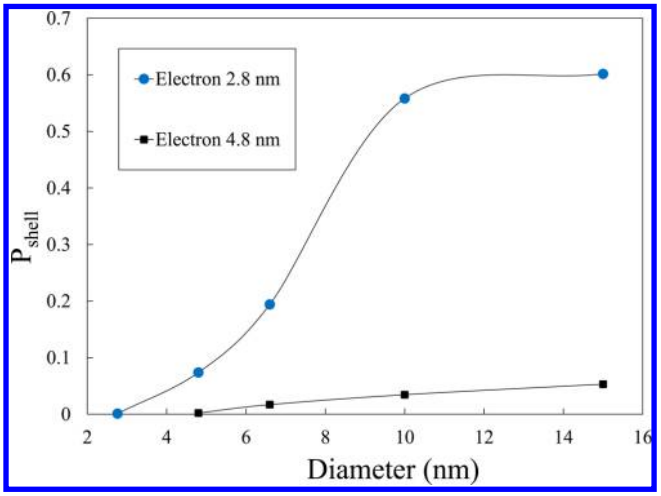

Figure 9. Relative probability (P_{shell}) of finding the electron in the shell region for CdSe/ZnS quantum dots with 2.8 and 4.8 nm CdSe core diameters.

energy of the core-only quantum dot was found to be 0.264 eV and is in good agreement with both experimental and theoretical findings for exciton binding energy.[56,122] For a factor of 3 increase in the dot diameter, the exciton binding energy was found to decrease by 46% in the core/shell dot.

In addition to the exciton binding energy, the electron−hole recombination probability was calculated from the eh-XCHF wave function using the following expression

$$P_{eh} = \frac{1}{N_e N_h} \int d\mathbf{r}_e \int_{\mathbf{r}_e-\Delta/2}^{\mathbf{r}_e+\Delta/2} d\mathbf{r}_h \rho_{eh}(\mathbf{r}_e, \mathbf{r}_h) \quad (15)$$

Analogous to the exciton binding energy, the recombination probability was found to decrease as the shell material was added to the CdSe core. As shown in Figure 2, the recombination probability decreased by 98% as compared to the bare CdSe QD. However, the change in the eh-recombination probability was much higher than the change in exciton binding energy.

The electron−hole separation distance r_{eh} was calculated as an additional metric for investigating the effect of shell thickness on the exciton dissociation process. The r_{eh} was calculated from the eh-XCHF wave function using the following expression

$$\langle r_{eh} \rangle = \langle \Psi_{eh-XCHF} \| \mathbf{r}_e - \mathbf{r}_h \| \Psi_{eh-XCHF} \rangle \quad (16)$$

and the results are presented in Figure 3. It is seen from Figure 3 that the spatial separation increases by 60% with the addition of ZnS shell.

The computational results presented in Figures 1−3 are consistent with experimental results on core/shell quantum dots. For example, in CdSe/ZnS QDs, Zhu et al. have found enhancement in the electron transfer rate from QDs with increasing shell thickness.[67] This phenomena is not restricted to CdSe/ZnS and is also seen in other core/shell quantum dots. Htoon et al. have shown an increase in multiexciton dissociation as a function of shell thickness.[130] In addition to core/shell QDs, exciton dissociation at the interface has also been observed in photoactive organic materials.[131−134]

3.2. Exponential Scaling with Respect to Shell Thickness. One of the interesting results in core/shell quantum dots is the exponential scaling of experimentally observed quantities as a function of shell thickness. In the present work, we find that as the shell thickness is increased, the recombination probability decays exponentially. Exponential fit of the relative recombination probability as a function of shell thickness is shown in Figure 4. These results are consistent with experimentally observed trends in core/shell quantum dots. For example, in 2010, Zhu et al. showed experimentally that there is an exponential decay associated with both charge-recombination and charge-transfer rates as a function of shell thickness.[67] Abdellah et al. have also found that the charge injection rate in core/shell quantum dots

Table 3. Scaling Equations for Core/Shell and Core-Only Quantum Dots[a]

Log[Property]	Log[E_{BE}/eV]		Log[P_{eh}]		Log[$\langle r_{eh} \rangle$/nm]	
scaling constants	m	c	m	c	m	c
2.8 nm core-diam.	−0.521	−0.147	−3.587	−14.875	0.487	−0.319
4.8 nm core-diam.	−0.569	−0.225	−3.730	−15.044	0.422	−0.202
core-only CdSe	−0.938	−0.004	−4.712	−13.308	0.809	−0.476

[a]Scaling relationships satisfy $A = m \log[D/nm] + c$, where A is the property being investigated.

DOI: 10.1021/ct500548x
J. Chem. Theory Comput. 2015, 11, 462−471

display a very strong exponential dependence.[68] Sun et al. found that the electron transfer rates in core/shell quantum dots show strong exponential decay with respect to increasing shell thickness.[135] Although in the present calculations a direct comparison with the rates are not possible, we find that similar trends exist between computed and experimentally observed quantities.

3.3. Preferential Localization of Quasiparticle Density. To further evaluate the spatial separation of the quasiparticles, we have computed the probability of finding the electron or hole in the core and shell region of the QD. Starting with the 1-particle reduced density, we define the probability P^{α}_{core} of finding the quasiparticle in the core region as

$$P^{\alpha}_{\text{core}} = \frac{1}{N_{\alpha}}\langle \rho_{\alpha}(\mathbf{r})\theta(r_{\text{core}} - |\mathbf{r}|)\rangle \tag{17}$$

$$= 1 - P^{\alpha}_{\text{shell}} \quad \text{with} \quad \alpha = \text{e, h} \tag{18}$$

where $\theta(x)$ is the Heaviside step function and the angular brackets represent integration over the spatial coordinates. The P_{shell} for both electron and hole are shown in Figure 5. It is seen that as compared to the hole, the electron is preferentially localized in the shell region by a factor of 3. This trend is consistent with experimental observations.[67−69,71,136−139] For example, Zhu et al. have found that there is an optimum shell thickness for controlling the charge separation in CdSe/ZnS QDs.[67] In addition, they have also observed preferential localization of the electron in the shell material for these QDs.[136] Abdellah et al. have also found that there is an optimal shell thickness for achieving efficient charge transfer from the core/shell quantum dot system.[68] As a consequence of this, core/shell quantum dots have been coupled with materials such as TiO_2 in order to modify the electron transfer rates.[71,137−139] Zhu et al. have engineered core/shell QDs to increase the charge separation and decrease the charge recombination.[69] The results in Figures 1−5 provide additional metrics that confirm these experimental observations.

3.4. Isolating the Effect of Heterojunction from Volume. The addition of multiple monolayers of shell material not only introduces heterojunction into the quantum dot but also increases the effective volume of the nanoparticle. It is often difficult to separate the influence of these two contributing quantities on the properties of the QD system. A useful metric to analyze these effects is to compute the scaling relationship of the excitonic properties as a function of the dot diameter. In this work, we isolate the effect of heterojunction by comparing the results between core/shell and core-only quantum dots with identical dot diameter.

The scaling of the exciton binding energy as a function of dot diameters was analyzed and is presented in Figure 6. The exciton binding energy for the CdSe/ZnS system was found to scale as $D_{\text{dot}}^{-0.56}$ with respect to the dot diameter D. This scaling behavior is considerably different from the scaling laws obtained in core-only quantum dots where the binding energy scaled as $D_{\text{dot}}^{-0.94}$.[55,122] We attribute this difference in the scaling behavior to the presence of the core/shell heterojunction. The scaling comparison for the core vs core−shell system was also evaluated for the eh-recombination probability and average eh-separation distance and the results from these calculations are presented in Figure 7 and Figure 8, respectively. In both cases, the scaling of the CdSe/ZnS properties was found to be different as compared to the core-only scaling. For P_{eh}, the core/shell system was found to scale as $D_{\text{dot}}^{-3.73}$ where the core-only system scaled as $D_{\text{dot}}^{-4.71}$. The average electron hole separation r_{eh} scaled as $D_{\text{dot}}^{0.42}$ for the core/shell system as compared to the $D_{\text{dot}}^{0.81}$ scaling exhibited in the core-only system. The significant deviation in the scaling behavior from the core-only QDs is consistent with experimental results reported earlier. García-Santamaría et al. found that core/shell quantum dots exhibit a breakdown in traditional volume scaling laws. They have shown that for a CdSe/CdS core/shell QD system with large shell thickness, the scaling laws associated with Auger recombination differ considerably from expected scaling.[140]

3.5. Effect of Core Size. To investigate the effect of the core size in core/shell QDs, we have generated a second set of CdSe/ZnS QDs with a smaller CdSe core-diameter of 2.8 nm. To facilitate direct comparison of excitonic properties between the two sets as a function of dot size, the dot diameters were selected to be identical to the first set of CdSe/ZnS dots with 4.8 nm core. The exciton binding energies for the CdSe/ZnS quantum dots with different core diameters are presented in Table 2. We find that, in all cases, the exciton binding energy of the CdSe/ZnS quantum dot with smaller core diameter is larger than that of the quantum dot with larger core diameter. The probability of finding the electron in the shell region as a function of dot size is shown in Figure 9. It was found that the core size can strongly influence the quasiparticle localization in the shell region. We find that in the 15 nm CdSe/ZnS quantum dot, reducing the size of the core by a factor of 1.7 increases the preferential localization of the electron in the shell region by a factor of 11.3. In contrast, the hole was found to be preferentially localized in the core with $P^{\text{h}}_{\text{core}}$ equal to 0.87 and 0.98 for the 15 nm CdSe/ZnS dot with 2.8 and 4.8 nm core-diameters, respectively. The results show that the hole density in the core is not substantially modified by the presence of the shell. These results are consistent with the experimental results on giant core/shell quantum dots, where dots with small cores were found to enhance multiexciton generation.[130]

The scaling of exciton binding energy, eh-recombination probability, and average eh-distance as a function of dot diameter for different core sizes and core-only dots are presented in Table 3. We find that both of the core/shell systems display similar scaling behavior with respect to dot size. However, as discussed earlier, the excitonic properties in core-only and core/shell dots exhibit different scaling behavior with respect to dot size, and we attribute the differences to the presence of heterojunction.

4. CONCLUSIONS

The goal of the present study was to investigate the effect of core/shell heterojunction on the excitonic properties of CdSe/ZnS quantum dots. The results from this study found that increasing the shell thickness in core/shell quantum dots could promote exciton dissociation by reducing the exciton binding energy and electron−hole recombination probability. The core/shell heterojunction was found to introduce spatial asymmetry in the 1-particle densities for the quasiparticles. Specifically, the electron was found to localize more in the shell region as compared to the hole. The results showed that the core/shell quantum dots follow different volume scaling laws for excitonic properties than the scaling laws followed by core-only quantum dots. Based on these observations, we conclude that the reduction in the exciton binding energy with increasing shell thickness cannot be attributed to only increasing volume alone and is a cumulative effect of presence of core/shell heterojunction and increasing volume.

DOI: 10.1021/ct500548x
J. Chem. Theory Comput. 2015, 11, 462−471

AUTHOR INFORMATION

Corresponding Author

*E-mail: archakra@syr.edu.

Notes

The authors declare no competing financial interest.

ACKNOWLEDGMENTS

We gratefully acknowledge financial support from Syracuse University and National Science Foundation (NSF) CAREER Award CHE-1349892. This work also used the Extreme Science and Engineering Discovery Environment (XSEDE), which is supported by National Science Foundation grant number ACI-1053575.

REFERENCES

(1) Midgett, A.; Luther, J.; Stewart, J.; Smith, D.; Padilha, L.; Klimov, V.; Nozik, A.; Beard, M. Size and Composition Dependent Multiple Exciton Generation Efficiency in PbS, PbSe, and PbS_xSe_{1-x} Alloyed Quantum Dots. *Nano Lett.* **2013**, *13*, 3078−3085.

(2) Eom, N.; Kim, T.-S.; Choa, Y.-H.; Kim, W.-B.; Kim, B. Core-Size-Dependent Properties of CdSe/CdS Core/Shell QDs. *Mater. Lett.* **2013**, *99*, 14−17.

(3) Yang, C.; Mai, Y.-W. Size-Dependent Absorption Properties of CdX (X = S, Se, Te) Quantum Dots. *Chem. Phys. Lett.* **2012**, *535*, 91−93.

(4) Li, H.; Brescia, R.; Povia, M.; Prato, M.; Bertoni, G.; Manna, L.; Moreels, I. Synthesis of Uniform Disk-Shaped Copper Telluride Nanocrystals and Cation Exchange to Cadmium Telluride Quantum Disks with Stable Red Emission. *J. Am. Chem. Soc.* **2013**, *135*, 12270−12278.

(5) Ren, P.; Xu, J.; Wang, Y.; Zhuang, X.; Zhang, Q.; Zhou, H.; Wan, Q.; Shan, Z.; Zhu, X.; Pan, A. Synthesis and Optical Properties of InP Quantum Dot/Nanowire Heterostructures. *Phys. Status Solidi A* **2013**, 1898−1902.

(6) Chen, L.; Gong, H.; Zheng, X.; Zhu, M.; Zhang, J.; Yang, S.; Cao, B. CdS and CdS/CdSe Sensitized ZnO Nanorod Array Solar Cells Prepared by a Solution Ions Exchange Process. *Mater. Res. Bull.* **2013**, *48*, 4261−4266.

(7) Yang, Z.-H.; Ullrich, C. Direct Calculation of Exciton Binding Energies with Time-Dependent Density-Functional Theory. *Phys. Rev. B* **2013**, *87*, 195204.

(8) Subila, K.; Kishore Kumar, G.; Shivaprasad, S.; George Thomas, K. Luminescence Properties of CdSe Quantum Dots: Role of Crystal Structure and Surface Composition. *J. Phys. Chem. Lett.* **2013**, *4*, 2774−2779.

(9) Liu, X.; Jiang, Y.; Fu, F.; Guo, W.; Huang, W.; Li, L. Facile Synthesis of High-Quality ZnS, CdS, CdZnS, and CdZnS/ZnS Core/Shell Quantum Dots: Characterization and Diffusion Mechanism. *Mater. Sci. Semicond. Process.* **2013**, *16*, 1723−1729.

(10) Beard, M.; Luther, J.; Semonin, O.; Nozik, A. Third Generation Photovoltaics Based on Multiple Exciton Generation in Quantum Confined Semiconductors. *Acc. Chem. Res.* **2013**, *46*, 1252−1260.

(11) Zhang, Y.; Ke, X.; Zheng, Z.; Zhang, C.; Zhang, Z.; Zhang, F.; Hu, Q.; He, Z.; Wang, H. Encapsulating Quantum Dots into Enveloped Virus in Living Cells for Tracking Virus Infection. *ACS Nano* **2013**, *7*, 3896−3904.

(12) Rakovich, A.; Nabiev, I.; Sukhanova, A.; Lesnyak, V.; Gaponik, N.; Rakovich, Y.; Donegan, J. Large Enhancement of Nonlinear Optical Response in a Hybrid Nanobiomaterial Consisting of Bacteriorhodopsin and Cadmium Telluride Quantum Dots. *ACS Nano* **2013**, *7*, 2154−2160.

(13) Wang, G.; Leng, Y.; Dou, H.; Wang, L.; Li, W.; Wang, X.; Sun, K.; Shen, L.; Yuan, X.; Li, J.; Sun, K.; Han, J.; Xiao, H.; Li, Y. Highly Efficient Preparation of Multiscaled Quantum Dot Barcodes for Multiplexed Hepatitis B Detection. *ACS Nano* **2013**, *7*, 471−481.

(14) Ji, X.; Palui, G.; Avellini, T.; Na, H.; Yi, C.; Knappenberger, K., Jr.; Mattoussi, H. On the pH-Dependent Quenching of Quantum Dot Photoluminescence by Redox Active Dopamine. *J. Am. Chem. Soc.* **2012**, *134*, 6006−6017.

(15) Draz, M.; Fang, B.; Li, L.; Chen, Z.; Wang, Y.; Xu, Y.; Yang, J.; Killeen, K.; Chen, F. Hybrid Nanocluster Plasmonic Resonator for Immunological Detection of Hepatitis B Virus. *ACS Nano* **2012**, *6*, 7634−7643.

(16) Smith, B.; Kempen, P.; Bouley, D.; Xu, A.; Liu, Z.; Melosh, N.; Dai, H.; Sinclair, R.; Gambhir, S. Shape Matters: Intravital Microscopy Reveals Surprising Geometrical Dependence for Nanoparticles in Tumor Models of Extravasation. *Nano Lett.* **2012**, *12*, 3369−3377.

(17) Zhang, Y.; Hong, G.; Zhang, Y.; Chen, G.; Li, F.; Dai, H.; Wang, Q. Ag_2S Quantum Dot: A Bright and Biocompatible Fluorescent Nanoprobe in the Second near-Infrared Window. *ACS Nano* **2012**, *6*, 3695−3702.

(18) Liu, S.-L.; Zhang, Z.-L.; Tian, Z.-Q.; Zhao, H.-S.; Liu, H.; Sun, E.-Z.; Xiao, G.; Zhang, W.; Wang, H.-Z.; Pang, D.-W. Effectively and Efficiently Dissecting the Infection of Influenza Virus by Quantum-Dot-Based Single-Particle Tracking. *ACS Nano* **2012**, *6*, 141−150.

(19) Jun, S.; Lee, J.; Jang, E. Highly Luminescent and Photostable Quantum Dot-Silica Monolith and Its Application to Light-Emitting Diodes. *ACS Nano* **2013**, *7*, 1472−1477.

(20) Maier-Flaig, F.; Rinck, J.; Stephan, M.; Bocksrocker, T.; Bruns, M.; Kübel, C.; Powell, A.; Ozin, G.; Lemmer, U. Multicolor Silicon Light-Emitting Diodes (SiLEDs). *Nano Lett.* **2013**, *13*, 475−480.

(21) Kwak, J.; Bae, W.; Lee, D.; Park, I.; Lim, J.; Park, M.; Cho, H.; Woo, H.; Yoon, D.; Char, K.; Lee, S.; Lee, C. Bright and Efficient Full-Color Colloidal Quantum Dot Light-Emitting Diodes Using an Inverted Device Structure. *Nano Lett.* **2012**, *12*, 2362−2366.

(22) Pal, B.; Ghosh, Y.; Brovelli, S.; Laocharoensuk, R.; Klimov, V.; Hollingsworth, J.; Htoon, H. Giant CdSe/CdS Core/Shell Nanocrystal Quantum Dots as Efficient Electroluminescent Materials: Strong Influence of Shell Thickness on Light-Emitting Diode Performance. *Nano Lett.* **2012**, *12*, 331−336.

(23) Zhao, J.; Holmes, M.; Osterloh, F. Quantum Confinement Controls Photocatalysis: A Free Energy Analysis for Photocatalytic Proton Reduction at CdSe Nanocrystals. *ACS Nano* **2013**, *7*, 4316−4325.

(24) Huang, J.; Mulfort, K.; Du, P.; Chen, L. Photodriven Charge Separation Dynamics in CdSe/ZnS Core/Shell Quantum Dot/Cobaloxime Hybrid for Efficient Hydrogen Production. *J. Am. Chem. Soc.* **2012**, *134*, 16472−16475.

(25) Ye, M.; Gong, J.; Lai, Y.; Lin, C.; Lin, Z. High-Efficiency Photoelectrocatalytic Hydrogen Generation Enabled by Palladium Quantum Dots-Sensitized TiO_2 Nanotube Arrays. *J. Am. Chem. Soc.* **2012**, *134*, 15720−15723.

(26) Wang, G.; Yang, X.; Qian, F.; Zhang, J.; Li, Y. Double-Sided CdS and CdSe Quantum Dot Co-Sensitized ZnO Nanowire Arrays for Photoelectrochemical Hydrogen Generation. *Nano Lett.* **2010**, *10*, 1088−1092.

(27) Alam, R.; Zylstra, J.; Fontaine, D. M.; Branchini, B. R.; Maye, M. M. Novel Multistep BRET-FRET Energy Transfer Using Nano-conjugates of Firefly Proteins, Quantum Dots, and Red Fluorescent Proteins. *Nanoscale* **2013**, *5*, 5303−5306.

(28) Snee, P. T.; Somers, R. C.; Nair, G.; Zimmer, J. P.; Bawendi, M. G.; Nocera, D. G. A Ratiometric CdSe/ZnS Nanocrystal pH Sensor. *J. Am. Chem. Soc.* **2006**, *128*, 13320−13321.

(29) Algar, W. R.; Ancona, M. G.; Malanoski, A. P.; Susumu, K.; Medintz, I. L. Assembly of a Concentric Forster Resonance Energy Transfer Relay on a Quantum Dot Scaffold: Characterization and Application to Multiplexed Protease Sensing. *ACS Nano* **2012**, *6*, 11044−11058.

(30) Stewart, M. H.; Huston, A. L.; Scott, A. M.; Efros, A. L.; Melinger, J. S.; Gemmill, K. B.; Trammell, S. A.; Blanco-Canosa, J. B.; Dawson, P. E.; Medintz, I. L. Complex Förster Energy Transfer Interactions between Semiconductor Quantum Dots and a Redox-Active Osmium Assembly. *ACS Nano* **2012**, *6*, 5330−5347.

(31) Nizamoglu, S.; Guzelturk, B.; Jeon, D.-W.; Lee, I.-H.; Demir, H. V. Efficient Nonradiative Energy Transfer from InGaN/GaN Nano-

DOI: 10.1021/ct500548x
J. Chem. Theory Comput. 2015, 11, 462−471

pillars to CdSe/ZnS Core/Shell Nanocrystals. *Appl. Phys. Lett.* **2011**, *98*, 163108.
(32) Ehrler, B.; Musselman, K.; Böhm, M.; Morgenstern, F.; Vaynzof, Y.; Walker, B.; MacManus-Driscoll, J.; Greenham, N. Preventing Interfacial Recombination in Colloidal Quantum Dot Solar Cells by Doping the Metal Oxide. *ACS Nano* **2013**, *7*, 4210−4220.
(33) Santra, P.; Kamat, P. Tandem-Layered Quantum Dot Solar Cells: Tuning the Photovoltaic Response with Luminescent Ternary Cadmium Chalcogenides. *J. Am. Chem. Soc.* **2013**, *135*, 877−885.
(34) Santra, P.; Kamat, P. Mn-Doped Quantum Dot Sensitized Solar Cells: A Strategy to Boost Efficiency Over 5%. *J. Am. Chem. Soc.* **2012**, *134*, 2508−2511.
(35) Genovese, M.; Lightcap, I.; Kamat, P. Sun-Believable Solar Paint. A Transformative One-Step Approach for Designing Nanocrystalline Solar Cells. *ACS Nano* **2012**, *6*, 865−872.
(36) Chang, L.-Y.; Lunt, R.; Brown, P.; Bulović, V.; Bawendi, M. Low-Temperature Solution-Processed Solar Cells Based on PbS Colloidal Quantum Dot/CdS Heterojunctions. *Nano Lett.* **2013**, *13*, 994−999.
(37) Žídek, K.; Zheng, K.; Abdellah, M.; Lenngren, N.; Chäbera, P.; Pullerits, T. Ultrafast Dynamics of Multiple Exciton Harvesting in the CdSe-ZnO System: Electron Injection versus Auger Recombination. *Nano Lett.* **2012**, *12*, 6393−6399.
(38) Tang, J.; Liu, H.; Zhitomirsky, D.; Hoogland, S.; Wang, X.; Furukawa, M.; Levina, L.; Sargent, E. Quantum Junction Solar Cells. *Nano Lett.* **2012**, *12*, 4889−4894.
(39) Pan, Z.; Zhang, H.; Cheng, K.; Hou, Y.; Hua, J.; Zhong, X. Highly Efficient Inverted Type-I CdS/CdSe Core/Shell Structure QD-Sensitized Solar Cells. *ACS Nano* **2012**, *6*, 3982−3991.
(40) Etgar, L.; Moehl, T.; Gabriel, S.; Hickey, S.; Eychmüller, A.; Grätzel, M. Light Energy Conversion by Mesoscopic PbS Quantum Dots/TiO_2 Heterojunction Solar Cells. *ACS Nano* **2012**, *6*, 3092−3099.
(41) Salant, A.; Shalom, M.; Tachan, Z.; Buhbut, S.; Zaban, A.; Banin, U. Quantum Rod-Sensitized Solar Cell: Nanocrystal Shape Effect on the Photovoltaic Properties. *Nano Lett.* **2012**, *12*, 2095−2100.
(42) Willis, S.; Cheng, C.; Assender, H.; Watt, A. The Transitional Heterojunction Behavior of PbS/ZnO Colloidal Quantum Dot Solar Cells. *Nano Lett.* **2012**, *12*, 1522−1526.
(43) Ehrler, B.; Wilson, M.; Rao, A.; Friend, R.; Greenham, N. Singlet Exciton Fission-Sensitized Infrared Quantum Dot Solar Cells. *Nano Lett.* **2012**, *12*, 1053−1057.
(44) Salant, A.; Shalom, M.; Hod, I.; Faust, A.; Zaban, A.; Banin, U. Quantum Dot Sensitized Solar Cells with Improved Efficiency Prepared Using Electrophoretic Deposition. *ACS Nano* **2010**, *4*, 5962−5968.
(45) Choi, H.; Ko, J.-H.; Kim, Y.-H.; Jeong, S. Steric-Hindrance-Driven Shape Transition in PbS Quantum Dots: Understanding Size-Dependent Stability. *J. Am. Chem. Soc.* **2013**, *135*, 5278−5281.
(46) Boehme, S.; Wang, H.; Siebbeles, L.; Vanmaekelbergh, D.; Houtepen, A. Electrochemical Charging of CdSe Quantum Dot Films: Dependence on Void Size and Counterion Proximity. *ACS Nano* **2013**, *7*, 2500−2508.
(47) Yang, Y.; Rodríguez-Córdoba, W.; Lian, T. Multiple Exciton Generation and Dissociation in PbS Quantum Dot-Electron Acceptor Complexes. *Nano Lett.* **2012**, *12*, 4235−4241.
(48) Cihan, A.; Hernandez Martinez, P.; Kelestemur, Y.; Mutlugun, E.; Demir, H. Observation of Biexcitons in Nanocrystal Solids in the Presence of Photocharging. *ACS Nano* **2013**, *7*, 4799−4809.
(49) Rabani, E.; Baer, R. Theory of Multiexciton Generation in Semiconductor Nanocrystals. *Chem. Phys. Lett.* **2010**, *496*, 227−235.
(50) Sukhovatkin, V.; Hinds, S.; Brzozowski, L.; Sargent, E. Colloidal Quantum-Dot Photodetectors Exploiting Multiexciton Generation. *Science* **2009**, *324*, 1542−1544.
(51) Rabani, E.; Baer, R. Distribution of Multiexciton Generation Rates in CdSe and InAs Nanocrystals. *Nano Lett.* **2008**, *8*, 4488−4492.
(52) Huang, J.; Huang, Z.; Yang, Y.; Zhu, H.; Lian, T. Multiple Exciton Dissociation in CdSe Quantum Dots by Ultrafast Electron Transfer to Adsorbed Methylene Blue. *J. Am. Chem. Soc.* **2010**, *132*, 4858−4864.
(53) Li, J.; Cushing, S. K.; Zheng, P.; Senty, T.; Meng, F.; Bristow, A. D.; Manivannan, A.; Wu, N. Solar Hydrogen Generation by a CdS-Au-TiO_2 Sandwich Nanorod Array Enhanced with Au Nanoparticle as Electron Relay and Plasmonic Photosensitizer. *J. Am. Chem. Soc.* **2014**, *136*, 8438−8449.
(54) Franceschetti, A.; Zunger, A. Direct Pseudopotential Calculation of Exciton Coulomb and Exchange Energies in Semiconductor Quantum Dots. *Phys. Rev. Lett.* **1997**, *78*, 915−918.
(55) Meulenberg, R. W.; Lee, J. R.; Wolcott, A.; Zhang, J. Z.; Terminello, L. J.; van Buuren, T. Determination of the Exciton Binding Energy in CdSe Quantum Dots. *ACS Nano* **2009**, *3*, 325−330.
(56) Jasieniak, J.; Califano, M.; Watkins, S. E. Size-Dependent Valence and Conduction Band-Edge Energies of Semiconductor Nanocrystals. *ACS Nano* **2011**, *5*, 5888−5902.
(57) Wang, L.-W.; Zunger, A. Pseudopotential Calculations of Nanoscale CdSe Quantum Dots. *Phys. Rev. B* **1996**, *53*, 9579−9582.
(58) Maan, J. C.; Belle, G.; Fasolino, A.; Altarelli, M.; Ploog, K. Magneto-Optical Determination of Exciton Binding Energy in GaAs−$Ga_{1-x}Al_xAs$ Quantum Wells. *Phys. Rev. B* **1984**, *30*, 2253−2256.
(59) Ramvall, P.; Tanaka, S.; Nomura, S.; Riblet, P.; Aoyagi, Y. Observation of Confinement-Dependent Exciton Binding Energy of GaN Quantum Dots. *Appl. Phys. Lett.* **1998**, *73*, 1104−1106.
(60) Blanton, C.; Brenon, C.; Chakraborty, A. Development of Polaron-Transformed Explicitly Correlated Full Configuration Interaction Method for Investigation of Quantum-Confined Stark Effect in GaAs Quantum Dots. *J. Chem. Phys.* **2013**, *138*, 054114.
(61) Rajadell, F.; Climente, J.; Planelles, J.; Bertoni, A. Excitons, Biexcitons, And Trions in CdSe Nanorods. *J. Phys. Chem. C* **2009**, *113*, 11268−11272.
(62) Qin, W.; Shah, R.; Guyot-Sionnest, P. CdSeS/ZnS Alloyed Nanocrystal Lifetime and Blinking Studies under Electrochemical Control. *ACS Nano* **2012**, *6*, 912−918.
(63) Verma, S.; Kaniyankandy, S.; Ghosh, H. Charge Separation by Indirect Bandgap Transitions in CdS/ZnSe Type-II Core/Shell Quantum Dots. *J. Phys. Chem. C* **2013**, *117*, 10901−10908.
(64) Wu, K.; Song, N.; Liu, Z.; Zhu, H.; Rodríguez-Córdoba, W.; Lian, T. Interfacial charge separation and recombination in InP and quasi-type II InP/CdS core/shell quantum dot-molecular acceptor complexes. *J. Phys. Chem. A* **2013**, *117*, 7561−7570.
(65) Xie, Y.-L. Enhanced Photovoltaic Performance of Hybrid Solar Cell Using Highly Oriented CdS/CdSe-Modified TiO_2 Nanorods. *Electrochim. Acta* **2013**, *105*, 137−141.
(66) Zhu, H.; Lian, T. Wavefunction Engineering in Quantum Confined Semiconductor Nanoheterostructures for Efficient Charge Separation and Solar Energy Conversion. *Energy Environ. Sci.* **2012**, *5*, 9406−9418.
(67) Zhu, H.; Song, N.; Lian, T. Controlling Charge Separation and Recombination Rates in CdSe/ZnS Type I Core-Shell Quantum Dots by Shell Thicknesses. *J. Am. Chem. Soc.* **2010**, *132*, 15038−15045.
(68) Abdellah, M.; Žídek, K.; Zheng, K.; Chábera, P.; Messing, M. E.; Pullerits, T. Balancing Electron Transfer and Surface Passivation in Gradient CdSe/ZnS Core−Shell Quantum Dots Attached to ZnO. *J. Phys. Chem. Lett.* **2013**, *4*, 1760−1765.
(69) Zhu, H.; Song, N.; Rodríguez-Córdoba, W.; Lian, T. Wave Function Engineering for Efficient Extraction of up to Nineteen Electrons from One CdSe/CdS Quasi-Type II Quantum Dot. *J. Am. Chem. Soc.* **2012**, *134*, 4250−4257.
(70) Xu, Z.; Hine, C. R.; Maye, M. M.; Meng, Q.; Cotlet, M. Shell Thickness Dependent Photoinduced Hole Transfer in Hybrid Conjugated Polymer/Quantum Dot Nanocomposites: From Ensemble to Single Hybrid Level. *ACS Nano* **2012**, *6*, 4984−4992.
(71) Hamada, M.; Nakanishi, S.; Itoh, T.; Ishikawa, M.; Biju, V. Blinking Suppression in CdSe/ZnS Single Quantum Dots by TiO_2 Nanoparticles. *ACS Nano* **2010**, *4*, 4445−54.
(72) Lee, M. H.; Geva, E.; Dunietz, B. D. Calculation from First Principles of Golden-Rule Rate Constants for Photo-Induced Subphthalocyanine/Fullerene Interfacial Charge Transfer and Re-

DOI: 10.1021/ct500548x
J. Chem. Theory Comput. 2015, 11, 462−471

combination in Organic Photovoltaic Cells. *J. Phys. Chem. C* **2014**, *118*, 9780−9789.
(73) Phillips, H.; Zheng, Z.; Geva, E.; Dunietz, B. D. Orbital Gap Predictions for Rational Design of Organic Photovoltaic Materials. *Org. Electron.* **2014**, *15*, 1509−1520.
(74) Wu, T.; Thompson, N.; Congreve, D.; Hontz, E.; Yost, S.; Van Voorhis, T.; Baldo, M. Singlet Fission Efficiency in Tetracene-Based Organic Solar Cells. *Appl. Phys. Lett.* **2014**, *104*.
(75) Troy Van Voorhis Yost, S.; Lee, J.; Wilson, M. W. B.; Wu, T.; McMahon, D. P.; Parkhurst, R. R.; Thompson, N. J.; Congreve, D. N.; Rao, A.; Johnson, K.; Sfeir, M. Y.; Bawendi, M. G.; Swager, T. M.; Friend, R. H.; Baldo, M. A.; Voorhis, T. V. A Transferable Model for Singlet-Fission Kinetics. *Nat. Chem.* **2014**, *6*, 492−497.
(76) Snoeberger, R.; Young, K.; Tang, J.; Allen, L.; Crabtree, R.; Brudvig, G.; Coppens, P.; Batista, V.; Benedict, J. Interfacial Electron Transfer into Functionalized Crystalline Polyoxotitanate Nanoclusters. *J. Am. Chem. Soc.* **2012**, *134*, 8911−8917.
(77) Nguyen, K.; Day, P.; Pachte. Understanding Structural and Optical Properties of Nanoscale CdSe Magic-Size Quantum Dots: Insight from Computational Prediction. *J. Phys. Chem. C* **2010**, *114*, 16197−16209.
(78) Yang, P.; Tretiak, S.; Ivanov, S. Influence of Surfactants and Charges on CdSe Quantum Dots. *J. Cluster Sci.* **2011**, *22*, 405−431.
(79) Albert, V.; Ivanov, S.; Tretiak, S.; Kilina, S. Electronic Structure of Ligated CdSe Clusters: Dependence on DFT Methodology. *J. Phys. Chem. C* **2011**, *115*, 15793−15800.
(80) Kilin, D.; Tsemekhman, K.; Prezhdo, O.; Zenkevich, E.; von Borczyskowski, C. Ab Initio Study of Exciton Transfer Dynamics from a Core−Shell Semiconductor Quantum Dot to a Porphyrin-Sensitizer. *J. Photochem. Photobiol., A* **2007**, *190*, 342−351.
(81) Liu, C.; Chung, S.-Y.; Lee, S.; Weiss, S.; Neuhauser, D. Adsorbate-Induced Absorption Redshift in an Organic−Inorganic Cluster Conjugate: Electronic Effects of Surfactants and Organic Adsorbates on the Lowest Excited States of a Methanethiol−CdSe Conjugate. *J. Chem. Phys.* **2009**, *131*, 174705.
(82) Chung, S.-Y.; Lee, S.; Liu, C.; Neuhauser, D. Structures and Electronic Spectra of CdSe-cys Complexes: Density Functional Theory Study of a Simple Peptide-Coated Nanocluster. *J. Phys. Chem. B* **2009**, *113*, 292−301.
(83) Kim, H.; Jang, S.-W.; Chung, S.; Lee, S.; Lee, Y.; Kim, B.; Liu, C.; Neuhauser, D. Effects of Bioconjugation on the Structures and Electronic Spectra of CdSe: Density Functional Theory Study of CdSe−Adenine Complexes. *J. Phys. Chem. B* **2010**, *114*, 471−479.
(84) Feng, Y.; Badaeva, E.; Gamelin, D. R.; Li, X. Excited-State Double Exchange in Manganese-Doped ZnO Quantum Dots: A Time-Dependent Density-Functional Study. *J. Phys. Chem. Lett.* **2010**, *1*, 1927−1931.
(85) Isborn, C. M.; Kilina, S. V.; Li, X.; Prezhdo, O. V. Generation of Multiple Excitons in PbSe and CdSe Quantum Dots by Direct Photoexcitation: First-Principles Calculations on Small PbSe and CdSe Clusters. *J. Phys. Chem. C* **2008**, *112*, 18291−18294.
(86) Noguchi, Y.; Sugino, O.; Nagaoka, M.; Ishii, S.; Ohno, K. A GW Bethe−Salpeter Calculation on Photoabsorption Spectra of (CdSe) 3 and (CdSe) 6 Clusters. *J. Chem. Phys.* **2012**, *137*, 024306.
(87) Lopez Del Puerto, M.; Tiago, M.; Chelikowsky, J. Ab initio methods for the optical properties of CdSe clusters. *Phys. Rev. B* **2008**, *77*, 045404.
(88) Del Puerto, M.; Tiago, M.; Chelikowsky, J. Excitonic Effects and Optical Properties of Passivated CdSe Clusters. *Phys. Rev. Lett.* **2006**, *97*, 096401.
(89) Neuhauser, D.; Rabani, E.; Baer, R. Expeditious Stochastic Calculation of Random-Phase Approximation Energies for Thousands of Electrons in Three Dimensions. *J. Phys. Chem. Lett.* **2013**, *4*, 1172−1176.
(90) Ge, Q.; Gao, Y.; Baer, R.; Rabani, E.; Neuhauser, D. A Guided Stochastic Energy-Domain Formulation of the Second Order Møller−Plesset Perturbation Theory. *J. Phys. Chem. L* **2013**, *5*, 185−189.
(91) Mazziotti, D.; Skochdopole, N. Functional Subsystems and Strong Correlation in Photosynthetic Light Harvesting. *Adv. Chem. Phys.* **2014**, *154*, 355−370.
(92) Skolnik, J.; Mazziotti, D. Cumulant Reduced Density Matrices As Measures of Statistical Dependence and Entanglement between Electronic Quantum Domains with Application to Photosynthetic Light Harvesting. *Phys. Rev. A* **2013**, *88*, 032517.
(93) Mazziotti, D. Effect of Strong Electron Correlation on the Efficiency of Photosynthetic Light Harvesting. *J. Chem. Phys.* **2012**, *137*.
(94) Foley, J.; Mazziotti, D. Measurement-Driven Reconstruction of Many-Particle Quantum Processes by Semidefinite Programming with Application to Photosynthetic Light Harvesting. *Phys. Rev. A* **2012**, *86*, 012512.
(95) Rothman, A.; Mazziotti, D. Variational Reduced-Density-Matrix Theory Applied to the Electronic Structure of Few-Electron Quantum Dots. *Phys. Rev. A* **2008**, *78*, 032510.
(96) Franceschetti, A.; Fu, H.; Wang, L. W.; Zunger, A. Many-Body Pseudopotential Theory of Excitons in InP and CdSe Quantum Dots. *Phys. Rev. B* **1999**, *60*, 1819−1829.
(97) Wang, L.-W.; Califano, M.; Zunger, A.; Franceschetti, A. Pseudopotential Theory of Auger Processes in CdSe Quantum Dots. *Phys. Rev. Lett.* **2003**, *91*, 056404.
(98) Baer, R.; Rabani, E. Communication: Biexciton Generation Rates in CdSe Nanorods Are Length Independent. *J. Chem. Phys.* **2013**, *138*, 051102.
(99) Elward, J. M.; Irudayanathan, F. J.; Nangia, S.; Chakraborty, A. Optical Signature of Formation of Protein Corona in the Firefly Luciferase−CdSe Quantum Dot Complex. *J. Chem. Theory Comput.* **2014**, *10*, 5524.
(100) Hu, Y. Z.; Lindberg, M.; Koch, S. W. Theory of Optically Excited Intrinsic Semiconductor Quantum Dots. *Phys. Rev. B* **1990**, *42*, 1713−1723.
(101) Zhu, X.; Hybertsen, M. S.; Littlewood, P. B. Electron−Hole System Revisited: A Variational Quantum Monte Carlo Study. *Phys. Rev. B* **1996**, *54*, 13575−13580.
(102) Burovski, E. A.; Mishchenko, A. S.; Prokofév, N. V.; Svistunov, B. V. Diagrammatic Quantum Monte Carlo for Two-Body Problems: Applied to Excitons. *Phys. Rev. Lett.* **2001**, *87*, 186402.
(103) Wimmer, M.; Nair, S. V.; Shumway, J. Biexciton Recombination Rates in Self-Assembled Quantum Dots. *Phys. Rev. B* **2006**, *73*, 165305.
(104) Woggon, U. *Optical Properties of Semiconductor Quantum Dots*; Springer Tracts in Modern Physics Vol. *136*; Springer-Verlag: Weinheim, 1997; p 252.
(105) Braskén, M.; Lindberg, M.; Sundholm, D.; Olsen, J. Full Configuration Interaction Calculations of Electron−Hole Correlation Effects in Strain-Induced Quantum Dots. *Phys. Status Solidi B* **2001**, *224*, 775−779.
(106) Corni, S.; Braskén, M.; Lindberg, M.; Olsen, J.; Sundholm, D. Stabilization Energies of Charged Multiexciton Complexes Calculated at Configuration Interaction Level. *Phys. E* **2003**, *18*, 436−442.
(107) Corni, S.; Braskén, M.; Lindberg, M.; Olsen, J.; Sundholm, D. Electron−Hole Recombination Density Matrices Obtained from Large Configuration-Interaction Expansions. *Phys. Rev. B* **2003**, *67*, 853141−853147.
(108) Corni, S.; Braskén, M.; Lindberg, M.; Olsen, J.; Sundholm, D. Size Dependence of the Electron−Hole Recombination Rates in Semiconductor Quantum Dots. *Phys. Rev. B* **2003**, *67*, 453131−453139.
(109) Vänskä, T.; Lindberg, M.; Olsen, J.; Sundholm, D. Computational Methods for Studies of Multiexciton Complexes. *Phys. Status Solidi B* **2006**, *243*, 4035−4045.
(110) Vänskä, T.; Sundholm, D. Interpretation of the Photoluminescence Spectrum of Double Quantum Rings. *Phys. Rev. B* **2010**, *82*, 085306.
(111) Sundholm, D.; Vänskä, T. Computational Methods for Studies of Semiconductor Quantum Dots and Rings. *Annu. Rep. Prog. Chem., Sect. C: Phys. Chem.* **2012**, *108*, 96−125.

DOI: 10.1021/ct500548x
J. Chem. Theory Comput. 2015, 11, 462−471

(112) Halonen, V.; Chakraborty, T.; Pietiläinen, P. Excitons in a Parabolic Quantum Dot in Magnetic Fields. *Phys. Rev. B* **1992**, *45*, 5980−5985.
(113) El-Said, M. Ground-State Energy of an Exciton in a Parabolic Quantum Dot. *Semicond. Sci. Technol.* **1994**, *9*, 272−274.
(114) Jaziri, S.; Bennaceur, R. Excitons in Parabolic Quantum Dots in Electric and Magnetic Fields. *Semicond. Sci. Technol.* **1994**, *9*, 1775−1780.
(115) Lamouche, G.; Fishman, G. Two Interacting Electrons in a Three-Dimensional Parabolic Quantum Dot: A Simple Solution. *J. Phys.: Condens. Matter* **1998**, *10*, 7857−7867.
(116) Xie, W.; Gu, J. Exciton Bound to a Neutral Donor in Parabolic Quantum Dots. *Phys. Lett. A* **2003**, *312*, 385−390.
(117) Xie, W. Exciton States Trapped by a Parabolic Quantum Dot. *Phys. B (Amsterdam, Neth.)* **2005**, *358*, 109−113.
(118) Xie, W. Effect of an Electric Field and Nonlinear Optical Rectification of Confined Excitons in Quantum Dots. *Phys. Status Solidi B* **2009**, *246*, 2257−2262.
(119) Karimi, M.; Rezaei, G. Effects of External Electric and Magnetic Fields on the Linear and Nonlinear Intersubband Optical Properties of Finite Semi-Parabolic Quantum Dots. *Phys. B (Amsterdam, Neth.)* **2011**, *406*, 4423−4428.
(120) Nammas, F.; Sandouqa, A.; Ghassib, H.; Al-Sugheir, M. Thermodynamic Properties of Two-Dimensional Few-Electrons Quantum Dot Using the Static Fluctuation Approximation (SFA). *Phys. B (Amsterdam, Neth.)* **2011**, *406*, 4671−4677.
(121) Rezaei, G.; Vaseghi, B.; Sadri, M. External Electric Field Effect on the Optical Rectification Coefficient of an Exciton in a Spherical Parabolic Quantum Dot. *Phys. B (Amsterdam, Neth.)* **2011**, *406*, 4596−4599.
(122) Elward, J. M.; Chakraborty, A. Effect of Dot Size on Exciton Binding Energy and Electron−Hole Recombination Probability in CdSe Quantum Dots. *J. Chem. Theory Comput.* **2013**, *9*, 4351−4359.
(123) Elward, J.; Thallinger, B.; Chakraborty, A. Calculation of Electron−Hole Recombination Probability Using Explicitly Correlated Hartree−Fock Method. *J. Chem. Phys.* **2012**, *136*, 124105.
(124) Elward, J. M.; Hoffman, J.; Chakraborty, A. Investigation of Electron−Hole Correlation Using Explicitly Correlated Configuration Interaction Method. *Chem. Phys. Lett.* **2012**, *535*, 182−186.
(125) Elward, J. M.; Hoja, J.; Chakraborty, A. Variational Solution of the Congruently Transformed Hamiltonian for Many-Electron Systems Using a Full-Configuration-Interaction Calculation. *Phys. Rev. A* **2012**, *86*, 062504.
(126) Bayne, M. G.; Drogo, J.; Chakraborty, A. Infinite-Order Diagrammatic Summation Approach to the Explicitly Correlated Congruent Transformed Hamiltonian. *Phys. Rev. A* **2014**, *89*, 032515.
(127) Swalina, C.; Pak, M. V.; Chakraborty, A.; Hammes-Schiffer, S. Explicit Dynamical Electron−Proton Correlation in the Nuclear-Electronic Orbital Framework. *J. Phys. Chem. A* **2006**, *110*, 9983−9987.
(128) Zhu, H.; Song, N.; Lian, T. Controlling Charge Separation and Recombination Rates in CdSe/ZnS Type I Core−Shell Quantum Dots by Shell Thicknesses. *J. Am. Chem. Soc.* **2010**, *132*, 15038−15045.
(129) Ghosh, P.; Ghosal, A.; Chattopadhyay, D. Magnetoelectronic Transport of the Two-Dimensional Electron Gas in CdSe Single Quantum Wells. *Pramana* **2009**, *72*, 399−405.
(130) Htoon, H.; Malko, A. V.; Bussian, D.; Vela, J.; Chen, Y.; Hollingsworth, J. A.; Klimov, V. I. Highly Emissive Multiexcitons in Steady-State Photoluminescence of Individual "Giant" CdSe/CdS Core/Shell Nanocrystals. *Nano Lett.* **2010**, *10*, 2401−2407.
(131) Yost, S.; Van Voorhis, T. Electrostatic Effects at Organic Semiconductor Interfaces: A Mechanism for "Cold" Exciton Breakup. *J. Phys. Chem. C* **2013**, *117*, 5617−5625.
(132) Difley, S.; Van Voorhis, T. Exciton/Charge-Transfer Electronic Couplings in Organic Semiconductors. *J. Chem. Theory Comput.* **2011**, *7*, 594−601.
(133) Lee, J.; Vandewal, K.; Yost, S.; Bahlke, M.; Goris, L.; Baldo, M.; Manca, J.; Voorhis, T. Charge Transfer State versus Hot Exciton Dissociation in Polymer−Fullerene Blended Solar Cells. *J. Am. Chem. Soc.* **2010**, *132*, 11878−11880.
(134) Zhu, X.-Y.; Yang, Q.; Muntwiler, M. Charge-Transfer Excitons at Organic Semiconductor Surfaces and Interfaces. *Acc. Chem. Res.* **2009**, *42*, 1779−1787 PMID: 19378979.
(135) Sun, J.; Zhao, J.; Masumoto, Y. Shell-thickness-dependent photoinduced electron transfer from $CuInS_2$/ZnS quantum dots to TiO_2 films. *Appl. Phys. Lett.* **2013**, *102*.
(136) Zhu, H.; Lian, T. Wavefunction Engineering in Quantum Confined Semiconductor Nanoheterostructures for Efficient Charge Separation and Solar Energy Conversion. *Energy Environ. Sci.* **2012**, *5*, 9406.
(137) Jin, S.; Lian, T. Electron Transfer Dynamics from Single CdSe/ZnS Quantum Dots to TiO_2 Nanoparticles. *Nano Lett.* **2009**, *9*, 2448−2454.
(138) Chang, C.-L.; Tsai, P.-Y.; Chang, Y.-p.; Lin, K.-C. Interfacial Electron Transfer from CdSe/ZnS Quantum Dots to TiO_2 Nanoparticles: Size Dependence at the Single-Molecule Level. *ChemPhysChem* **2012**, *13*, 2711−2720.
(139) Choi, H.; Santra, P. K.; Kamat, P. V. Synchronized Energy and Electron Transfer Processes in Covalently Linked CdSe-Squaraine Dye-TiO_2 Light Harvesting Assembly. *ACS Nano* **2012**, *6*, 5718−5726.
(140) García-Santamaría, F.; Brovelli, S.; Viswanatha, R.; Hollingsworth, J. A.; Htoon, H.; Crooker, S. A.; Klimov, V. I. Breakdown of Volume Scaling in Auger Recombination in CdSe/CdS Heteronanocrystals: The Role of the Core−Shell Interface. *Nano Lett.* **2011**, *11*, 687−693.

DOI: 10.1021/ct500548x
J. Chem. Theory Comput. 2015, 11, 462−471